Colloidal Gel Filtration: Experiment and Theory

Charlton Shen and William B. Russel
Dept. of Chemical Engineering, Princeton University, Princeton, NJ 08544

François M. Auzerais
Schlumberger-Doll Research, Ridgefield, CT 06877

The filtration of colloidal gels, consisting of octadecyl-coated silica spheres in hexadecane, is examined experimentally using CAT scanning. A number of interparticle strengths are explored, with significant differences in qualitative behavior relative to the filtration of stable dispersions. For stiff gels, the transmission of stresses from the cell wall to the dispersion results in a fracturing phenomenon during consolidation on a length scale substantially larger than the particle size. For more pliant gels, the radial propagation of stress is more local to the wall region and gravitational effects play a prominent role. The existing theory of network consolidation is compared against our experimental results for pliant gels, independent of the form of the constitutive functions for the sedimentation velocity and yield stress. Though our measurements seem consistent with the theory at early times, deviations at later moments question whether a compressive yield stress is actually present.

Introduction

Many industrial processes rely on the separation and manipulation of micron-sized particulates dispersed in viscous liquids. The most readily understood situation is of particles without an appreciable affinity for one another. This situation is not always realized, however. The flocculation of particles into aggregates or gel-like networks complicates the processing of a variety of materials including foods, soils, ceramic powders, and chemical/biological waste products. Though many materials of technological interest exist in a flocculated state, a fundamental understanding of the connection between the processing and properties of flocculated materials remains elusive.

Investigations have attempted to qualify and quantify the properties of flocculated dispersions in a variety of contexts, both fundamental and applied in perspective. Most concern sedimentation processes. One of the earliest works, by Coe and Clevenger (1916), documented the various regimes of sedimentation in slime-settling tanks. In a more quantitative and systematic study, Michaels and Bolger (1962) argued that floc, as opposed to particle, size controls sedimentation and correlated the final depth of the sediment with the initial concentration of solids. Following Kynch's (1952) explanation of sedimentation for stable dispersions, Shin and Dick (1980) measured the flux curve for flocculated calcium carbonate systems dispersed in aqueous solutions at various particle concentrations, while Fitch (1983) adapted the analysis to account for the effects of a compressible sediment.

Focusing attention on consolidation of networked dispersions reveals that one of the earliest descriptions is Terzaghi's (1948) classic work in soil mechanics, applied by Yagi and Yamazaki (1960) to compressible sediments. Related contributions include Gibson, England, and Hussey's (1967) general one-dimensional model of soil consolidation under finite strains, solved numerically by Lee and Sills (1981) with network stresses and permeabilities varying linearly with void fraction. Their model assumes that the coefficient of consolidation, defined by:

$$C_F = \frac{k(1-\phi)^3}{\rho_f}\frac{d\sigma}{d\phi}$$

is constant, where k is the permeability, σ is the particle stress, ρ_f is the fluid density, and ϕ is the solids volume fraction. The experiments of Been and Sills (1981), utilizing pressure meas-

Correspondence concerning this article should be addressed to W. B. Russel.

urements along the wall of a settling column, confirmed the model to some extent.

Researchers studying the settling of slurries in batch and continuous thickeners also contributed substantially. Gaudin et al. (1959) established the presence and qualitative effects of network formation above the sediment. Tory and Shannon (1965) emphasized that the rate and final state of compression depend upon both the total weight of solids above a plane of consolidation and the local solids concentration at that plane. Shirato et al. (1970) combined experiment and theory to establish a constitutive relation between the fractional pore volume and particle stress. Kos (1977) extended the constitutive equation to depend upon the particle stress gradient as well. Tiller and Khatib (1984) developed a theory which predicts the final sediment height, assuming that the local porosity depends on the buoyant weight of solids, height of the sediment, and intrinsic particle characteristics.

The most recent models (Buscall and White, 1987; Auzerais et al., 1988) establish a comprehensive treatment of flocculated network consolidation. The models are essentially identical; a continuum theory uniquely predicts the solids volume fraction, ϕ, and the fluid and solid velocities at all positions and times. The basic elements include generalized continuity and momentum equations written for both phases and phenomenological constitutive equations relating particle stress and sedimentation velocity to volume fraction. The central tenet is that the gel possesses a compressive yield stress, that is, consolidation occurs only if $\sigma \geq \sigma_y(\phi)$. Buscall and White's formulation was solved by Howells et al. (1988) and Landman et al. (1988) to depict the transients during consolidation under gravity. Experimental testing of the model for sedimentation of flocculated systems by Auzerais et al. (1990) met with limited success. Bergström (1992) recently applied the model to flocculated alumina suspensions, probed via gamma-ray attenuation. His results included a correlation of the compressive yield stress with volume fraction and interparticle potential. However, he noted that the model fails to predict the densification observed above the sediment and that the standard constitutive equations underpredict the permeability at low volume fractions; the previous results of Been and Sills support the former observation.

The filtration of flocculated materials has received less attention than sedimentation, but has not been completely ignored. For example, Lange and Miller (1987) and Massuda et al. (1988) focused on weakly flocculated dispersions that form compressible filter cakes. Also, Buscall and White's model applies to the filtration of networks both strong and weak (Landman et al., 1991; Landman and Russel, 1993), as discussed more thoroughly later in our exposition. In general, the need for a systematic experimental study of flocculated dispersion filtration persists in order to qualify and improve existing theoretical work, especially for dispersions initially in a gel state.

Our objective is to present experimental work involving the pressure filtration of strongly flocculated suspensions of spherical organophilic silica particles dispersed in hexadecane. Here, strongly flocculated refers to an initial gel possessing a compressive yield stress comparable to or greater than the self-weight of the dispersion. Our experiments vary particle size, applied pressure, temperature, and initial particle concentration in order to assess the effect of each. X-ray computer-assisted tomography (CAT scanning) yields two-dimensional concentration mappings during the filtration process. Finally, the model proposed by Buscall and White is interpreted in a manner allowing a direct comparison with our pliant experiments. The model captures the early time behavior but substantial deviations arise later.

Model Colloidal System

Studying flocculated suspensions necessitates control over the particle shapes, sizes, distributions, and interparticle potential, as well as compatibility with the analytical devices that detect their physical properties. Matijević (1985) reviewed a number of model colloidal systems synthesized for various purposes.

Silica spheres, coated with a dense layer of octadecyl chains, are ideal for our studies (Chen and Russel, 1992). The synthesis is fairly straightforward and produces a relatively monodisperse distribution of spherical particles with an average size ranging from 0.05 to 1.0 μm, depending upon the reaction conditions. The synthesis proceeds by Stöber's method (1968). The grafting of octadecyl chains on the surface, which imparts the organophilic nature, follows a method patented by Iler and described later (1979). A number of workers have verified the full surface coverage by grafted chains using elemental analysis to calculate the average surface area occupied per chain (Van Helden et al., 1981; Emmett et al., 1989).

A substantial effort towards understanding how reactant concentrations and conditions affect particle size and size distribution has been made (Van Helden et al., 1981; Tan et al., 1987; Bogush et al., 1988; Badley et al., 1990; Harris et al., 1990). Variations on the Stöber method yield denser particles by adding acetic acid to the reaction broth (Karmakar et al., 1991) and a more uniform distribution for smaller sizes using a reverse-micellar technique (Osseo-Asare and Arriagada, 1990). More uniform, larger particles can be achieved by seeded growth (Bogush et al., 1988; Coenen and de Kruif, 1988). Earlier, many hypothesized particle formation to follow the short-time nucleation model of LaMer and Dinegar (1950). For example, Matsoukas and Gulari (1988, 1989) proposed a simplified monomer addition model, essentially a modified LaMer and Dinegar model, to explain their experimental results for growth kinetics. More recently, however, Bogush and Zukoski (1991a,b) proposed an aggregative growth model which explains evidence that conflicts with the LaMer and Dinegar model (Harris et al., 1990; Look et al., 1990; Bogush and Zukoski, 1991a). Kim and Zukoski (1990) have also suggested a detailed model for seeded growth via heterocoagulation accounting for electostatic, dispersion, and Brownian induced forces. Their conclusions include the unimportance of hydrodynamic interactions under a wide range of reaction conditions and the tendency of seeded systems to become more monodisperse.

The three batches of silica particles used in experiments described here were synthesized according to the methods described by Van Helden et al. (1981) and Post (1985). Our approach deviated from previous syntheses only in the extraction of excess octadecanol upon completion of surface grafting. For particles with diameters smaller than 0.2 μm, ethanol and cyclohexane were added to the grafting dispersion upon reaction completion to increase the solubility of octadecanol and prevent its freezing during centrifugation. All

subsequent centrifugations were performed with pure cyclohexane. Table 1 summarizes the average particle size measured by dynamic light scattering (DLS) and transmission electron microscopy (TEM), the apparent particle densities, and the concentrations of reactants in the particle syntheses for the two batches of interest here. Apparent particle densities were determined by taking a known weight of particles, with known weight of solvent, and filling a volumetric flask to a specific volume. Particles were dried under vacuum before weighing to insure an accurate measurement. For all particles synthesized, the values range from 1.71 to 2.02 g/mL and are consistent with those determined by others (Auzerais, 1988; Bogush et al., 1988; Davis, 1989). Since amorphous silica has a density of 2.2 g/mL, the particles must be porous, as noticed by others (Lecloux et al., 1986).

The interactions of octadecyl chains with a specific dispersion media at a particular temperature establishes the interparticle potential. We chose hexadecane as the solvent for our experiments from a variety of different ones explored by Jansen et al. (1986). In hexadecane below 29°C, an attraction between particles induces a strong, but reversible, flocculation that creates a volume-filling gel at solids volume fractions as low as 0.05 (Chen, 1992). Dispersions in this state possess a compressive yield stress; thus, a finite force is necessary to consolidate the material. Raising the temperature above 29°C disperses the gel, creating a fluid dispersion that becomes more stable as the temperature is increased. For small particles, the dispersion is hard sphere like at high temperatures. For particles greater than 0.3 μm, however, a simple calculation shows that the energy associated with London-van der Waals attractions becomes comparable to thermal energy. Thus a state of aggregation persists for larger particles in hexadecane at temperatures well above the gel-transition temperature. Other coatings lead to different particle-particle interactions (Cosgrove et al., 1988; Pathmamanoharan, 1988/89; Philipse and Vrij, 1989; van Duijneveldt and Beysens, 1991).

The exact nature of the interparticle potential is not well understood. For larger particles, the London-van der Waals attractions are appreciable beyond contact of the octadecyl layers. Superimposed upon this and dominant for smaller particles is a short-range force of ambiguous nature that induces the gel transition. deKruif and van Miltenburg (1990) in their study of particles dispersed in toluene hypothesize an order-disorder transition due to the grafted chain layer freezing at the gel-transition temperature. No definitive explanation exists, however. Other studies of silica particles grafted with hydrocarbon chains include Vrij et al. (1990), who delineated the spinodal with pulse-induced critical light scattering, and Chen and Russel (1991, 1993), who defined the gelation transition using static light scattering and linear viscoelastic measurements. Both correlated the data with the adhesive hard sphere model of Baxter (1968).

X-Ray Scanning with Computer-Assisted Tomography

X-ray CAT scanning provides a nonintrusive, quantitatively accurate technique to extract two-dimensional atomic and bulk density mappings. The technique was rapidly developed for medical applications in the early 1970s with the first operating machine created by EMI Limited in England. The basic principle involves detecting the attenuation of photons from a subject at various angles with the source and detectors shifted in a synchronous manner. The data is used to mathematically reconstruct a two-dimensional cross-section of the object. Applications of the technique to colloidal systems include Tjipangandjara et al.'s (1990) study of sedimenting alumina, with adsorbed polyacrylic acid controlling the flocculation through pH, and Auzerais et al.'s (1990) study of sedimentation in stable and flocculated silica dispersions.

Our experiments were performed with an Elsinct 2002 Bimodal CT scanner, owned by Schlumberger-Doll Research Laboratory. Photons are produced by a continuous radiation, stationary anode tube, operated at 140 kV and 43 mA to optimize image contrast while minimizing large photon energy fluctuations. The translate-rotate method of scanner operation is chosen to maximize image resolution. In this mode, an X-ray source traverses an object five times averaging data over a width of three millimeters, while 279 $CdWO_4$ detectors collecting intensity data at various angles are sampled 512 times per traverse. The scanner at Schlumberger has been modified to run at "half-speed," providing twice the sampling per traverse and increased image resolution.

Since photon scattering or absorption is a single event process (Evans, 1955), attenuation is truly exponential in nature. Thus, the scattered intensity of a well-collimated beam of photons obeys Beer's law:

$$\ln\left(\frac{I}{I_o}\right) = -\int \mu(x, y)ds$$

where I and I_o are the transmitted and initial intensities, respectively, μ is the linear attenuation coefficient, and s is the coordinate along the path. This relationship holds for any particular angle, with μ dependent upon the energy of the photons and the atomic and bulk densities of the material. The mathematics of reconstruction involves solving the above integral equation for a mapping of μ in the plane of interest; the problem is essentially an inversion. We do not pursue the

Table 1. Particle Synthesis Data

Particle Batch	Apparent Density (g/mL)	Synthesis Data (TEOS)	Synthesis Data (NH_3)	Total Vol. (mL)	d_{DLS} (μm)	TEM Data d_{TEM} (μm)	TEM Std. Dev. (μm)	No. of Part. Sized
I	1.74	0.18	1.10	4,500	0.357	0.255	0.047	142
II	1.73	0.18	0.80	4,000	0.133	0.116	0.015	237
III	1.76	0.30	0.687	6,000	0.310	0.182	0.047	95

details here but refer the interested reader elsewhere (Cormack, 1973; Brooks and DiChiro, 1976).

Though photons interact with atoms in four ways, with three possible effects of the interactions, most events are either Compton scattering or a photoelectric effect between photons and outer shell atomic electrons. Compton scattering occurs when an incident photon has momentum comparable to the target electron, resulting in deflection of the photon with some transfer of momentum to the electron. In the photoelectric effect, a photon of smaller momentum is completely absorbed by strongly bound electrons and a photoelectron is ejected to conserve momentum.

Since scattering is a single event process, μ is a sum of the two described contributions:

$$\mu = \mu_p + \mu_c \quad \text{with} \quad \mu_p = \alpha \frac{Z^{3.8}}{E^{3.2}} \rho \qquad \mu_c = \beta \rho$$

where μ_p is the photoelectric contribution (Wellington and Vinegar, 1987), μ_c is the Compton contribution, ρ is the bulk density of the material, Z is the effective atomic number of the material, and α and β are energy dependent constants. For the range of photon energy fluctuations generated by the CAT scanner, however, α and β are effectively taken as constants. Formally, the attenuation coefficients are proportional to the electron density. However, since Z/A is roughly the same for most elements, with Z the number of electrons per atom and A the atomic weight, the proportionality with bulk density holds. At 140 kV, the Compton contribution should dominate, leaving μ directly proportional to the bulk density.

Figure 1 shows a calibration curve relating solids volume fraction with CT number, a normalized attenuation coefficient defined by:

$$\text{CT number} = \text{CT}_o + 1{,}000 \frac{\mu_m - \mu_r}{\mu_r}$$

where μ_m is the measured attenuation coefficient, μ_r is the attenuation coefficient for a reference material and CT_o is an offset value. We prepared several samples of known solids volume fraction, ϕ, and scanned them to obtain the attenuation. The fit of the data demonstrates the dominance of Compton scattering and serves as our calibration, associating any CT number with a volume fraction.

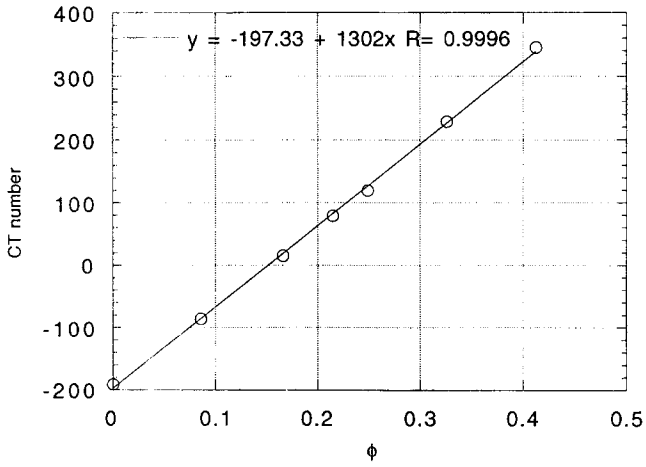

Figure 1. Calibration curve: CT number vs. solids volume fraction.

The calibration experiment also defines the accuracy of our measurements from the fluctuations in average intensity. The accuracy depends on whether the data is radially averaged or raw, the former case being ± 0.010 in solids volume fraction while the latter is ± 0.015. For the results presented here, radial concentration gradients prevent averaging. Spatially, the scanner resolves position to within ± 0.5 mm, though the resolution decreases when the atomic or bulk densities are similar for two adjacent materials.

Since the photon source is not monochromatic, large and extended fluctuations in energy may occur. Such a fluctuation would invalidate our calibration curve since attenuation depends upon the photon energy. To detect such fluctuations, a sample of pure hexadecane is placed next to the filtration cell during each scan. Deviations of attenuation from the point $\phi = 0$ on the calibration curve indicate an energy fluctuation and invalidate that data. This was a rare event in our experiments.

Experimental Equipment

Numerous considerations constrained the design of a pressure filtration cell for our experiments. Pressures of hundreds of kilopascals were found necessary to drive fluids through filter cakes of closed-packed submicron particles within one to two days. Additionally, the filtration apparatus must not attenuate X-rays strongly while resisting chemical attack from the organic solvents of interest. Finally, temperature control is necessary since the interparticle potential is a strong function of temperature.

Two cells were constructed, as depicted in Figure 2: one capable of sustaining pressures to 690 kPa and the other rated to over 1,380 kPa. The cell wall is polyether sulfone (ICI Americas) with nylon flanges (Nylatron GSM, Plastics Center, Conshohocken, PA) and stainless steel threaded rods for support. The inner wall is coated with teflon to minimize gel adherence. The steel rods do not attenuate X-rays since they do not intersect the plane of photon propagation. A nylon disk with several thousand holes, each approximately 1/50 cm in diameter, sufficed for the filter support. Filter membranes of nylon, teflon, or cellulose nitrate (MFS and Cole Parmer), with pore sizes from 0.1 μm to 0.5 μm, retain flocs; a thin cloth of teflon (Zitex A, LEM Plastics, Wallington, NJ) spread over the membrane acted as a prefilter to guard against particle adhesion. An outer wall of polycarbonate created an annular region to hold water circulated from a constant temperature bath controlled to within ± 0.1°C. Nitrogen, supplied by a port at the top, created a pressure head that drove liquid flow. Fittings and lines, for both nitrogen and effluent, were either nylon or teflon in construction (Swaglock and Cole Parmer).

Experimental Procedures and Conditions

The filtration experiments were conducted at a constant applied pressure and constant temperature with the CAT scanner taking images at designated times. Reconstructed images produced by the scanner were transferred into a binary format

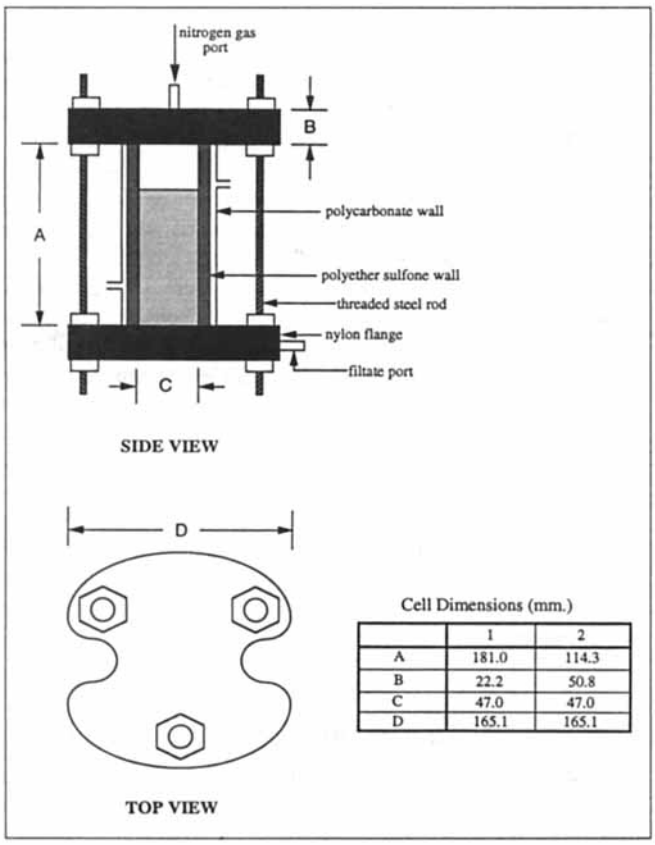

Figure 2. Pressure-filtration cell and dimensions.

and downloaded for analysis using KBVision, an image analysis software package. Since imaging requires approximately one minute and an experiment lasts hours to days, we obtained essentially instantaneous solid fraction profiles of the process. The flux of fluid removed is measured with a scale and checked against the flux derived from interfacial heights measured by the scanner; measurements typically agree within 2% of each other. Different experiments vary temperature, pressure, particle size, and initial particle concentration.

Initial conditions were difficult to establish consistently since flocculated materials exist in a nonequilibrium state. The procedure followed involves sonicating a dispersion at a temperature well above its gel point, pouring the dispersion into the cell at the temperature desired, and waiting for thermal equilibrium. A thermal steady state was achieved after one and a half hours, based on a calculation for heat conduction in a cylindrical geometry with the materials of interest (Carslaw and Jaeger, 1959). In the strongly flocculated experiments, establishing a uniform initial concentration of particles at a particular temperature proved difficult when the yield stress was smaller than the self-weight of the gel; this was often the case when using particles larger than 0.3 μm in size. The slight axial volume fraction gradient initially present in most experiments, however, was probably an artifact of aspect ratio disfiguring from image reconstruction and not due to sedimentation during the dispersion cooling period. The only exception is for Experiment A.

Table 2. Experimental Parameters

Experiment	Δp (kPa)	Temp. (°C)	Particle Batch	d (μm)	ϕ_o	Type
A	828	25	I	0.36	0.16	pliant
B	621	22	I	0.36	0.11	pliant
C	828	27	II	0.13	0.10	stiff
D	1380	27	II	0.13	0.13	stiff
E	345	22.1	III	0.31	0.10	N/A

Results

Preliminary comments

When a dispersion exists in a gel state, filtration differs qualitatively from that for a typical stable suspension. The existence of an interparticle contact stress transmits forces up from the bottom further hindering consolidation and slowing filtration. Additionally, the strong particle-particle interactions can propagate shear stresses from the walls and produce radial and axial gradients within the gel region and the filter cake. We divide the results of this section under two headings: *pliant systems and stiff systems*. For *pliant systems* the gravitational forces exceed the compressive yield stress of the initial gel, $\sigma_y(\phi_o)$, that is, $\sigma_y(\phi_o)/\Delta\rho g H_o\phi_o < 1$, with $\Delta\rho$ the density difference between the solid and liquid, g the gravitational acceleration, H_o the initial height of the dispersion, and ϕ_o the initial volume fraction. If $\sigma_y(\phi_o)/\Delta\rho g H_o\phi_o \geq 1$, we label the system *stiff*. The various experimental cases studied are outlined in Table 2.

A sense of the process time-scale for consolidation of gels can be obtained from a comparison with those for the sedimentation and filtration of stable dispersions. Figure 3 depicts a column for sedimentation or filtration, with H, y, and L marking the positions of the interfaces. Assuming uniform densities for all regions between the interfaces, a material balance on the solid phase has the form:

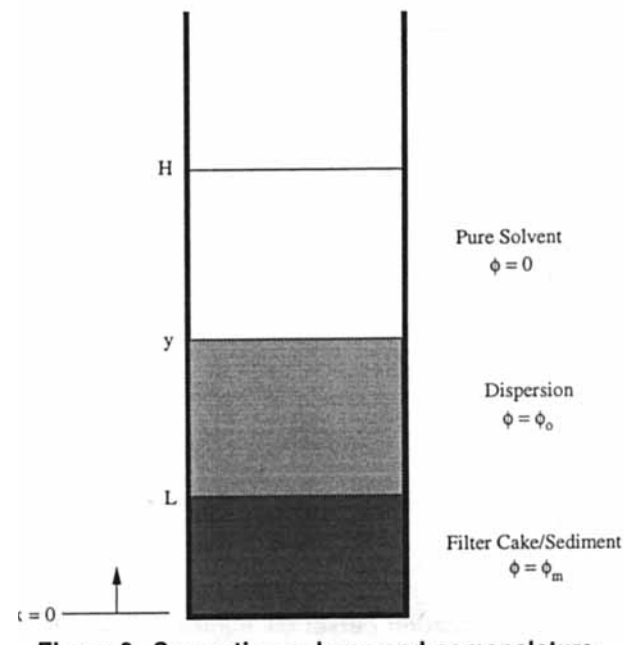

Figure 3. Separation column and nomenclature.

$$\phi_o H_o = \phi_o (y - L) + \phi_m L = \phi_m L_f \tag{1}$$

with ϕ_m the final packing volume fraction and L_f the final cake height.

In the case of sedimentation, the no-flux boundary condition on the fluid requires that $H = H_o$ at all times. Thus the rate of descent of y is simply the solids velocity:

$$\frac{dy}{dt} = -U_o K(\phi_o) \tag{2}$$

with U_o the Stokes velocity of an isolated sphere and $K(\phi_o)$ the hindered settling coefficient. Integrating Eq. 2 with Eq. 1 yields the height of the sediment growing as a function of time:

$$\frac{L}{L_f} = \frac{t}{t_{\text{sed}}} \quad \text{with} \quad t_{\text{sed}} = \frac{\phi_m - \phi_o}{\phi_m} \frac{H_o}{U_o K(\phi_o)} \tag{3}$$

t_{sed} denoting the time to pack all the particles in a sediment of height L_f.

For filtration of a stable dispersion at a constant pressure, the physical situation entails fluid motion sweeping particles along at the same rate. Thus the velocity of liquid equals the solids and the y and H interfaces coincide at all times. The fluid velocity, given by Darcy's law, equals the rate of descent of the H interface:

$$\frac{dH}{dt} = -\frac{k \Delta p}{\eta L} \quad \text{with} \quad k = \frac{2a^2}{75} \frac{(1 - \phi_m)^3}{\phi_m^2} \tag{4}$$

In the above expressions, k is the permeability of the cake, specified directly by the Blake-Kozeny equation, η is the solvent viscosity, Δp is the applied pressure, and a is an individual particle radius. A check between the permeability predicted by the Blake-Kozeny equation and direct measurements from our experiments, at $\phi = \phi_m$, shows agreement to within 10%. Solving these equations predicts the height of the filter cake as a function of time as:

$$\frac{L}{L_f} = \sqrt{\frac{t}{t_{\text{filt}}}} \quad \text{with} \quad t_{\text{filt}} = \frac{\eta H_o^2}{2k \Delta p} \frac{\phi_o (\phi_m - \phi_o)}{\phi_m^2} \tag{5}$$

Thus L grows as $t^{1/2}$ and reaches its final height at $t = t_{\text{filt}}$, which sets the filtration time-scale.

Table 3 documents the time-scales associated with our experimental conditions. In calculating t_{sed}, $K(\phi)$ is chosen equal to one, giving a minimum time for stable sedimentation. Clearly sedimentation is not significant for stable dispersions at our experimental conditions. Additionally, these values provide a basis for assessing the effects of flocculation on filtration processes.

Table 3. Experimental Time-Scales

Experiment	t_{sed}	t_{filt}
A	625 h	2.64 h
B	798 h	6.08 h
C	311 d	52.1 h
D	253 d	28.4 h

Pliant systems

The initial gel of both experiments examined in this section was not completely uniform due to sedimentation during the thermal equilibration period. Thus a small region of pure solvent appeared above each dispersion before compression began. For Experiment A, a substantial axial volume fraction differential of 0.04 from top to bottom exists at the beginning of compression. The initial gradient maintains its integrity throughout the experiment. An initial scan of Experiment B shows a considerably smaller gradient which is probably an artifact from image reconstruction.

Experiment A shows the typical features observed for pliant, strongly flocculated systems. Figure 4 depicts the various stages of filtration along with the corresponding vertical density profiles at three radial positions: centerline, intermediate zone, and near the cell wall. A clear zone grows on top of the dispersion in the early stage of filtration with a jagged interface separating the gel from the pure solvent. Transmission of stresses from the cell wall causes the interface to bend. A dense filter cake begins forming immediately after pressure is introduced, with a solids volume fraction quickly approaching the random closed-packing value of $\phi = 0.64$. For all strongly flocculated experiments, the filter cakes were essentially incompressible with no detectable strain recovery witnessed upon the relief of applied pressure and only slight densification during filtration.

As the experiment proceeds, a cup-like depression forms on top of the gel in the center of the tube and grows deeper with time. The gel close to the wall, however, does not fall faster than the solvent. This might reflect the absence of thermal equilibrium before compression began, though calculations indicate the equilibration time should have been sufficient. Visual observations indicate that some gel adheres to the wall as the pure solvent/gel interface moves downward. The total amount, however, does not reduce the total mass of gel by more than 5% in all cases.

Gel consolidation slows substantially as the gel approaches complete compaction into the growing filter cake: the gas/pure solvent interface in the center begins closing on the pure solvent/gel interface instead of moving away from it. Concurrently, an axial gradient develops near the surface of the filter cake. Early in the experiment, the cake interface is fairly flat, but at later stages depressions develop at the cell wall. This may be attributed to the quicker consolidation of gel in the center, as supported by the cup-like formation and its increasing depth with time. Finally, the liquid region disappears and the remaining gel consolidates into the filter cake. The final cake surface is not flat and has a small crown near, but not directly adjacent to, the wall.

The solid fraction profiles associated with Figure 4 indicate little radial dependence, with the exception of the cup-like depression. The jagged nature of the profiles arises from both the precision of the measurement and the heterogeneous nature of the gel, that is, fluctuations of high and low density probably indicate the heterogeneous nature of clustering in the gel. The profile associated with Figure 4d reveals an axially uniform final filter cake, except close to the cake surface where a small gradient appears. Figure 5 superimposes profiles at several different instances in the center of the cell. The plot shows the gel region maintaining the small initial axial gradient without further densification with time. Note that in all solid fraction

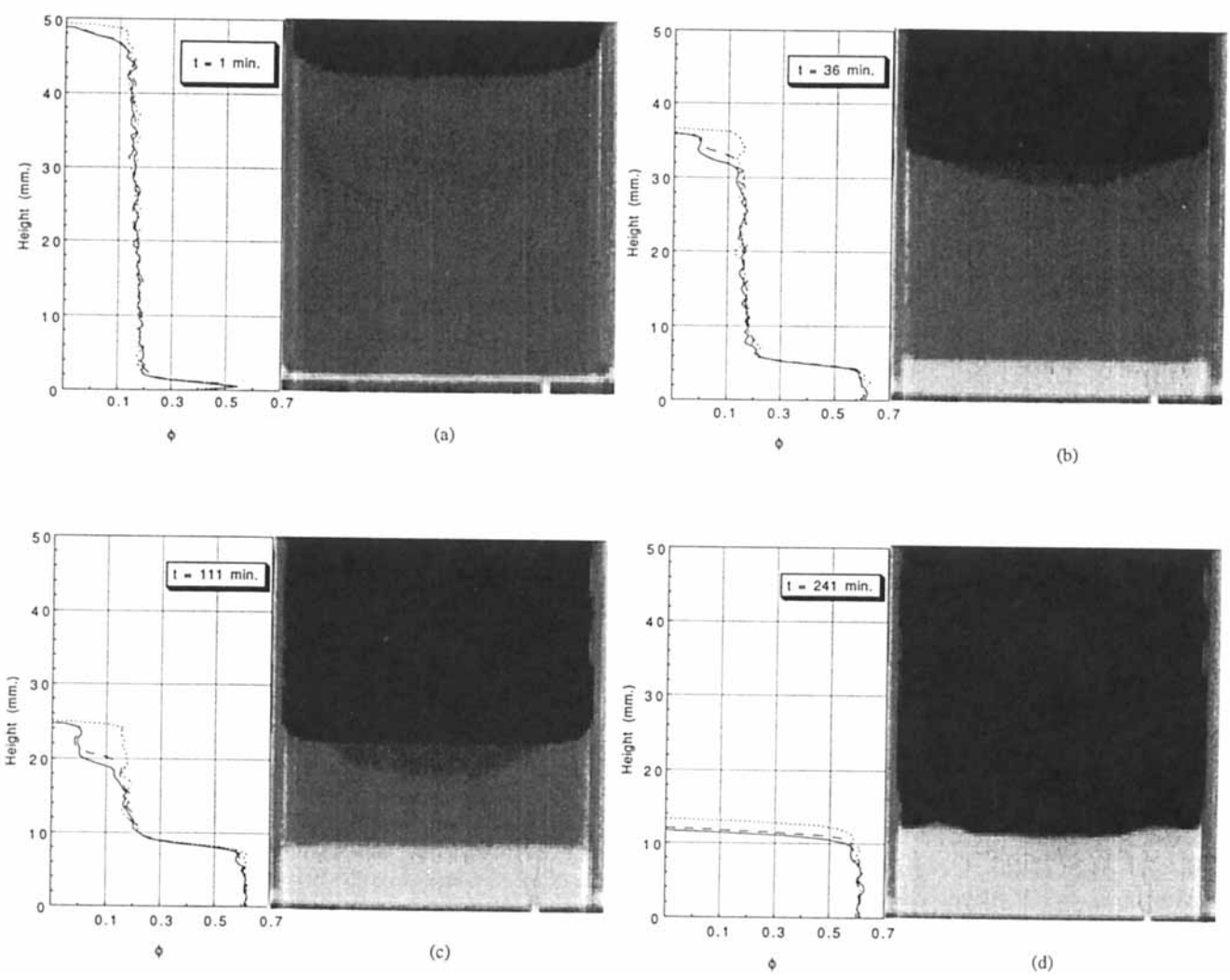

Figure 4. Reconstructed images and associated solid fraction profiles for Experiment A.

— $r/R = 0.000$; - - - - $r/R = 0.377$; · · · · $r/R = 0.755$; where r/R is the ratio of the radial position to the tube radius.

profile plots, the regions with gas only have a density lower than the pure solvent's, hence the profiles show values of ϕ less than zero.

Figure 6 plots the centerline interfacial heights as functions of time, with the heights scaled on H_o and time on t_{filt}. Early during filtration, the top interface drops as $1/t^{1/2}$ while a filter cake grows as $t^{1/2}$, in accord with stable dispersions. However, an interface quickly develops between the gel and clear solvent, denoted by y. Clearly at early times $-dy/dt$ is greater than $-dH/dt$ in magnitude, indicating that solids move at a higher velocity than liquid. At later times, however, it is clear that $-dy/dt$ decreases in magnitude toward zero while dH/dt becomes roughly constant, so that y and H converge before reaching the filter cake surface, L. Figure 7 reinforces this point: the difference height, $H-y$, vs. time passes through a maximum, showing the reversal in relative velocity between the two interfaces.

Additional conclusions may be drawn from Figures 6 and 7 by examining the scaling of the plots. If the dispersion were stable for Experiment A, H and y would essentially track each other in Figure 6 and meet L, growing as $t^{1/2}$, at $t/t_{filt} = 1$, terminating filtration. However, Experiment A requires 50% more time for completion. The slope of Figure 7 yields the difference velocity between the solid and liquid phases at the y interface. With the scaling on H_o for height and on H_o/U_o for time, a slope of unity would indicate a difference velocity equal to the Stokes settling velocity. The initial slope of $O(10^2)$ indicates why sedimentation affects this process; though $t_{filt}/t_{sed} \ll 1$ with $K(\phi_o) = 1$, in the experiment $K(\phi_o)$ is actually much larger than unity. $K(\phi)$ is actually misnamed as a *hindered* settling coefficient here since flocculation *enhances* the settling rate. Certainly other flocs hinder a particular floc's sedimentation relative to being alone in an infinite space. $K(\phi)$, however, measures the floc velocity relative to that of an individual particle, U_o. Here the enhancement due to cluster formation greatly outweighs the retardation. Thus, our hypothesis is that gravitational forces are responsible for the clear liquid region, which increases the rate of solids consolidation and, therefore, the overall process time. Additionally, overcoming the network stress imposes another force which extends the time to completion.

Experiment B, involving another pliant system, differs from Experiment A since the concentration of particles and the dispersion temperature are lower. The behavior also differs,

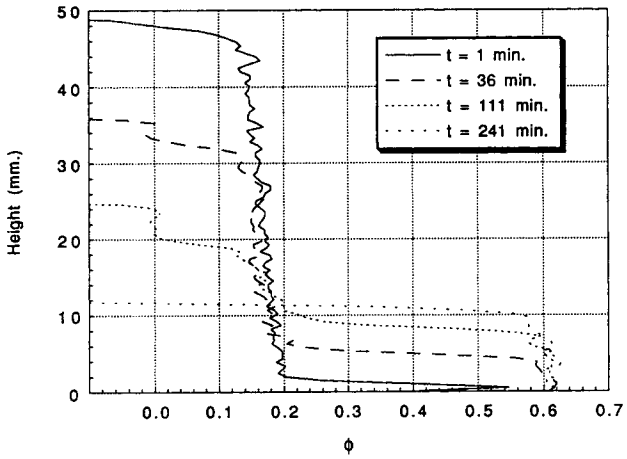

Figure 5. Centerline solid fraction profiles at various times for Experiment A.

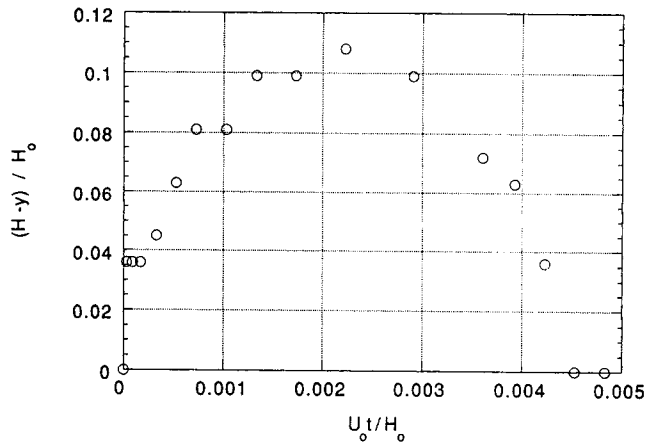

Figure 7. Scaled graph of difference height vs. time at centerline for Experiment A.

as depicted in Figure 8. Again, a curved interface forms between clear hexadecane and gel. In this instance, however, the clear liquid extends radially to the cell wall and a cloudy interface separates the gel and liquid, as opposed to the central depression and distinct interface observed in the previous experiment. Again the gel interface slows upon approaching the filter cake, with an axial gradient in concentration developing in the gel. The cake forms a depression around the cell wall with a crown at the edge of the depression.

The associated concentration profiles show a new feature. At later times during the experiment, the gel region adjacent to the cell wall densifies with time, in contrast to the centerline and intermediate radial positions which essentially track one another. The observation indicates the presence of a radial gradient and is consistent with the fact that gel closer to the wall has a more difficult time being compressed into the filter cake due to the transmission of stresses from the wall. Figure 9 again shows the axial densification of the gel with time along the centerline, with slightly more pronouncement near the cell wall (data not shown).

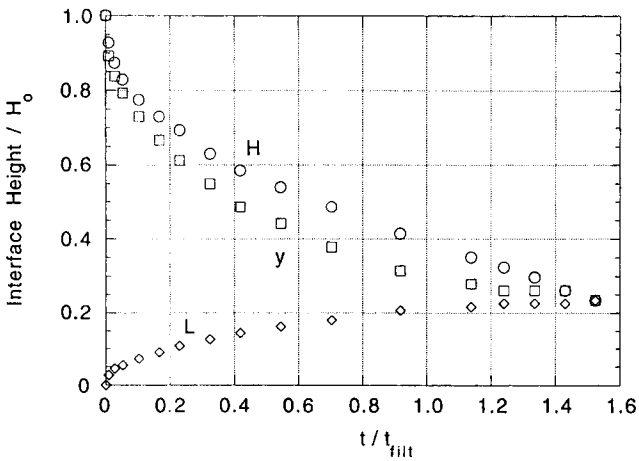

Figure 6. Scaled graph of interface height vs. time at centerline for Experiment A.

A plot of the centerline interfacial heights vs. time, Figure 10, repeats many of the features of Figure 6. Although this experiment was not run to completion, the slow approach of the y interface to the filter cake is apparent. As well, the extension of the process time relative to the stable case accords with Experiment A. The difference height plot, Figure 11, is also consistent, with a smaller initial slope, $K(\phi_o) \approx 60$, and higher maximum.

Stiff systems

Stiff gels consolidate differently from their pliant counterparts owing to the larger magnitude of the compressive yield stress relative to the self-weight of the gel, $\Delta\rho g H_o \phi_o$. These experiments, involving gels with larger yield stresses, were carried out with smaller particles at higher temperatures; the factor of three decrease in particle-size results in more interparticle contacts, apparently increasing the yield stress over the decrease resulting from a shallower potential minimum at higher temperatures. Consequently, these experiments require more time to complete, lasting days as opposed to hours.

Experiment C shows many of the features witnessed in these systems, as depicted by Figure 12. Unlike the pliant systems, no clear liquid region forms above the gel before filtration begins. For the first two-and-a-half hours, compression of the gel forms a filter cake with a significant axial concentration gradient and a maximum solids fraction, ϕ_m, not exceeding 0.66. The increase in maximum solids fraction packing is probably due to the slight polydispersity of the particles. As well, radial gradients develop early in the gel region. This contrasts with the pliant systems, which did not develop measurable differences until late in the process.

After three hours, fractures occur within the gel: many small radial ones along the wall and a large one in the center, though the poor resolution of the reproduced image hides the features. These fractures appear to close with time while new ones form. This fracture/consolidation mode continues throughout the experiment. Concurrently, a liquid region forms above the gel and grows, Figure 12b, while the difference velocity decreases monotonically, Figure 13. The liquid/gel interface, more defined relative to the pliant experiment observations, develops a curvature due to radial stresses transmitted from the wall.

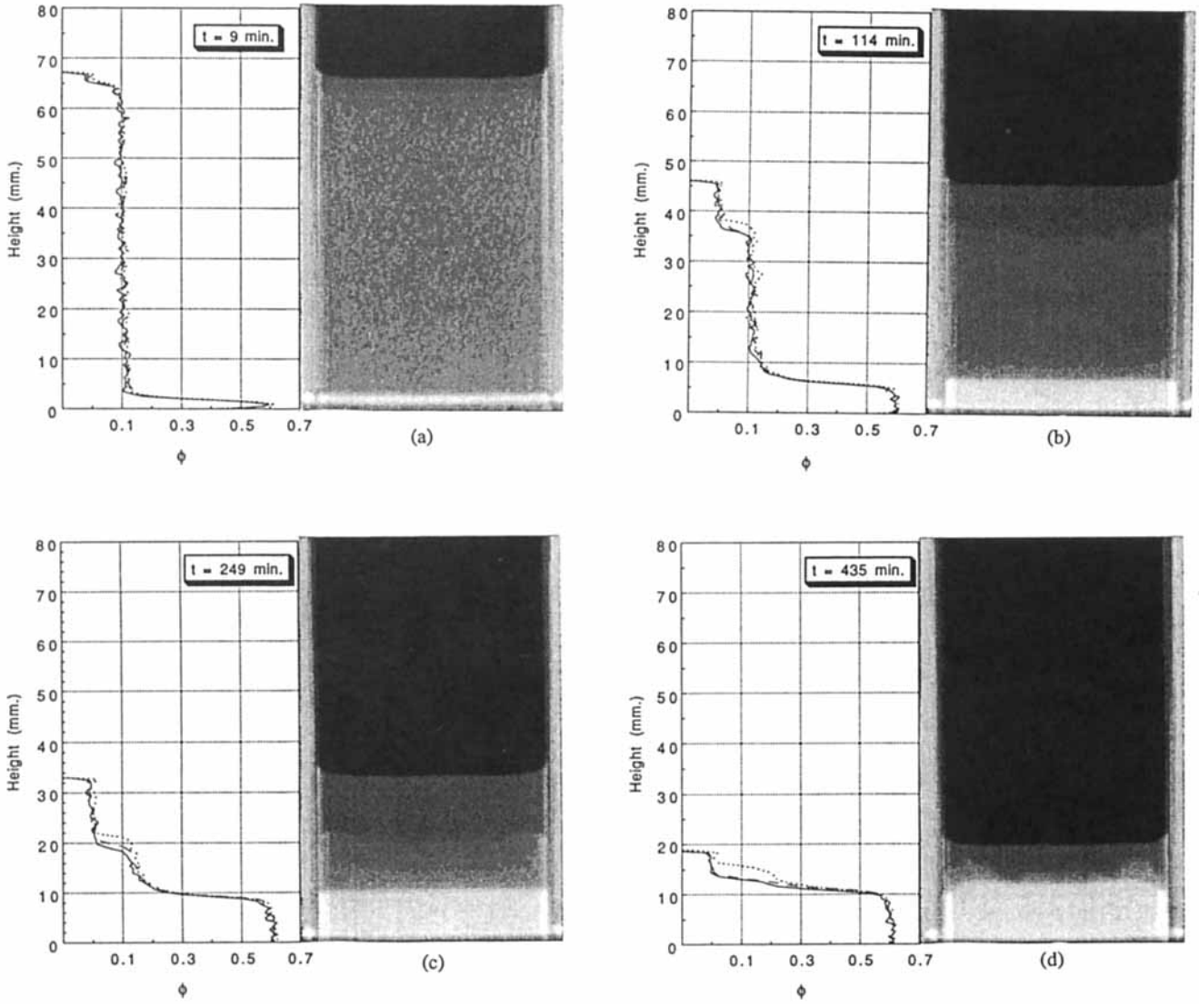

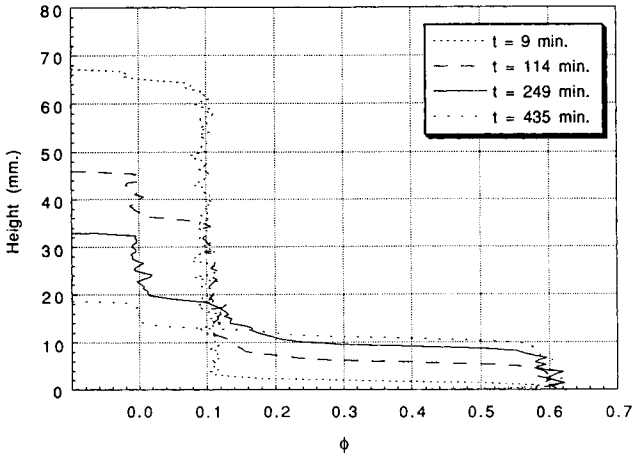

Figure 9. Centerline solid fraction profiles at various times for Experiment B.

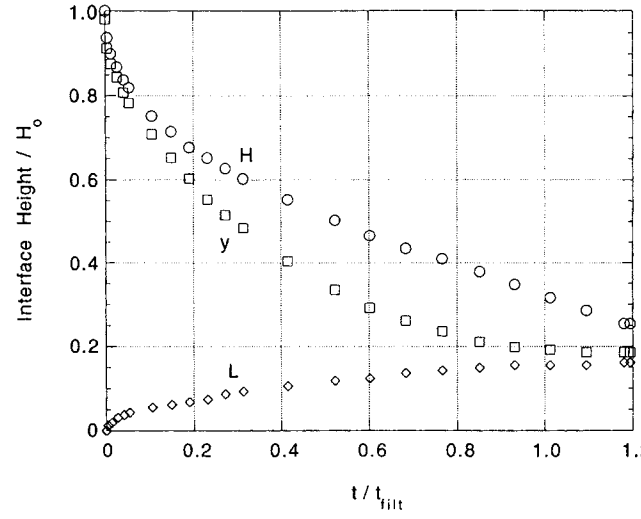

Figure 10. Scaled graph of interface height vs. time at centerline for Experiment B.

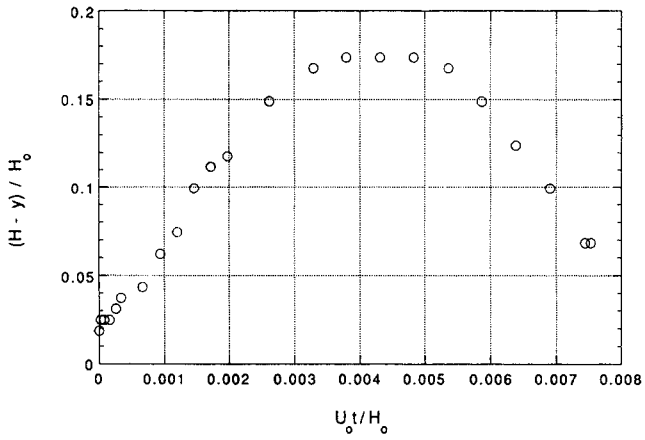

Figure 11. Scaled graph of difference height vs. time at centerline for Experiment B.

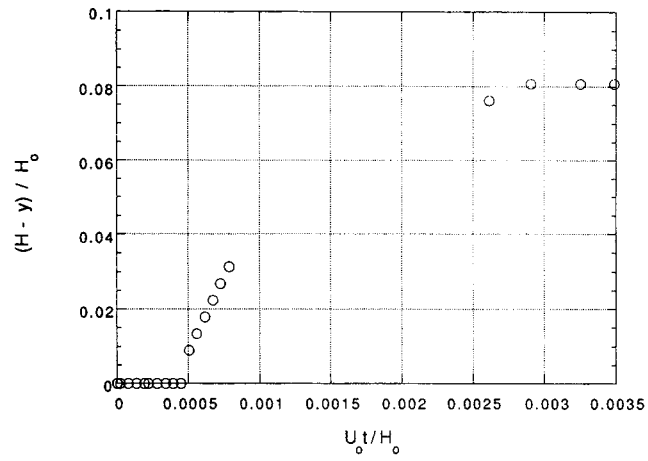

Figure 13. Scaled graph of difference height vs. time at centerline for Experiment C.

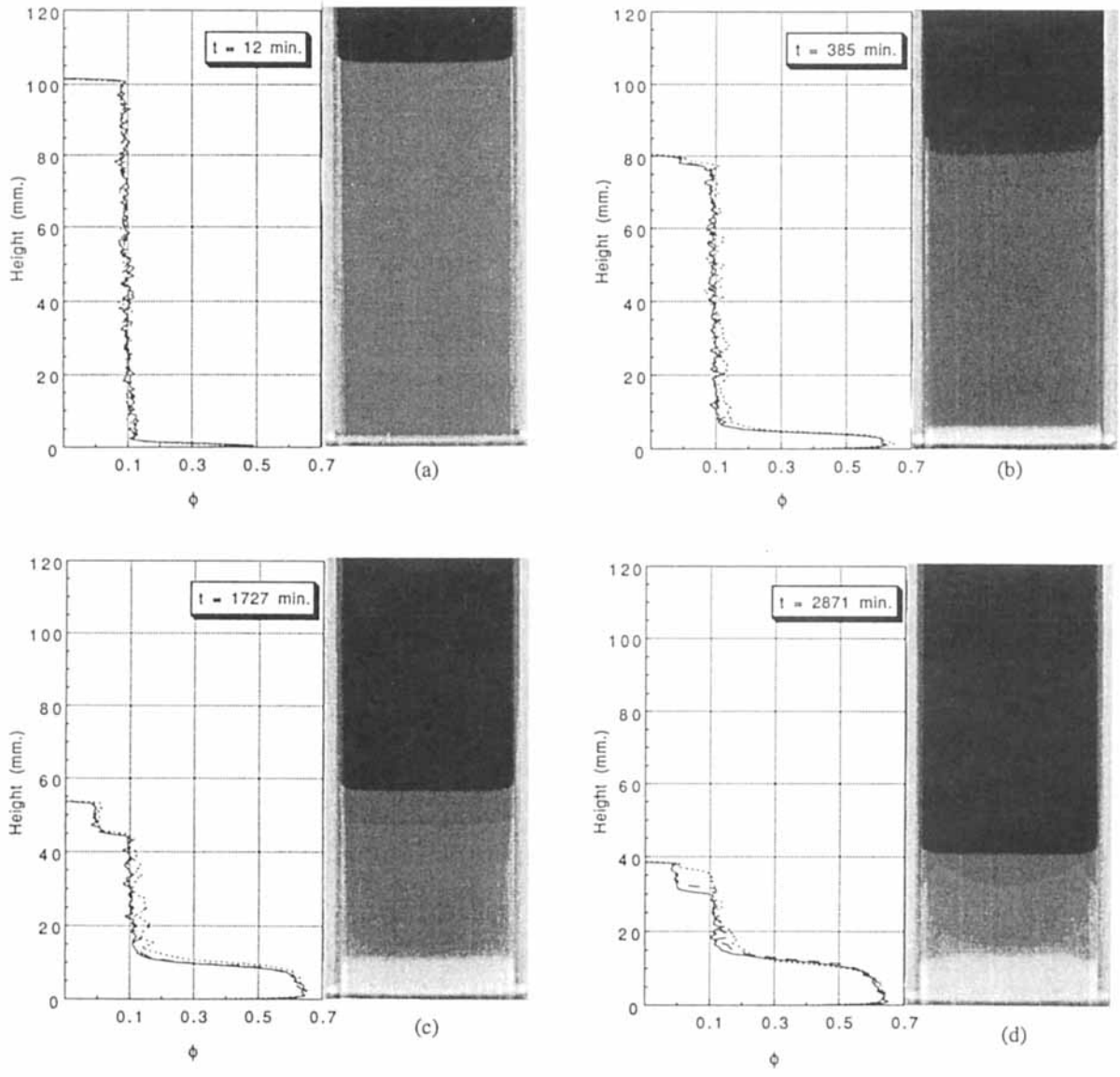

Figure 12. Reconstructed images and associated solid fraction profiles for Experiment C.

— $r/R = 0.000$; - - - - $r/R = 0.354$; · · · · $r/R = 0.708$; where r/R is the ratio of the radial position to the tube radius.

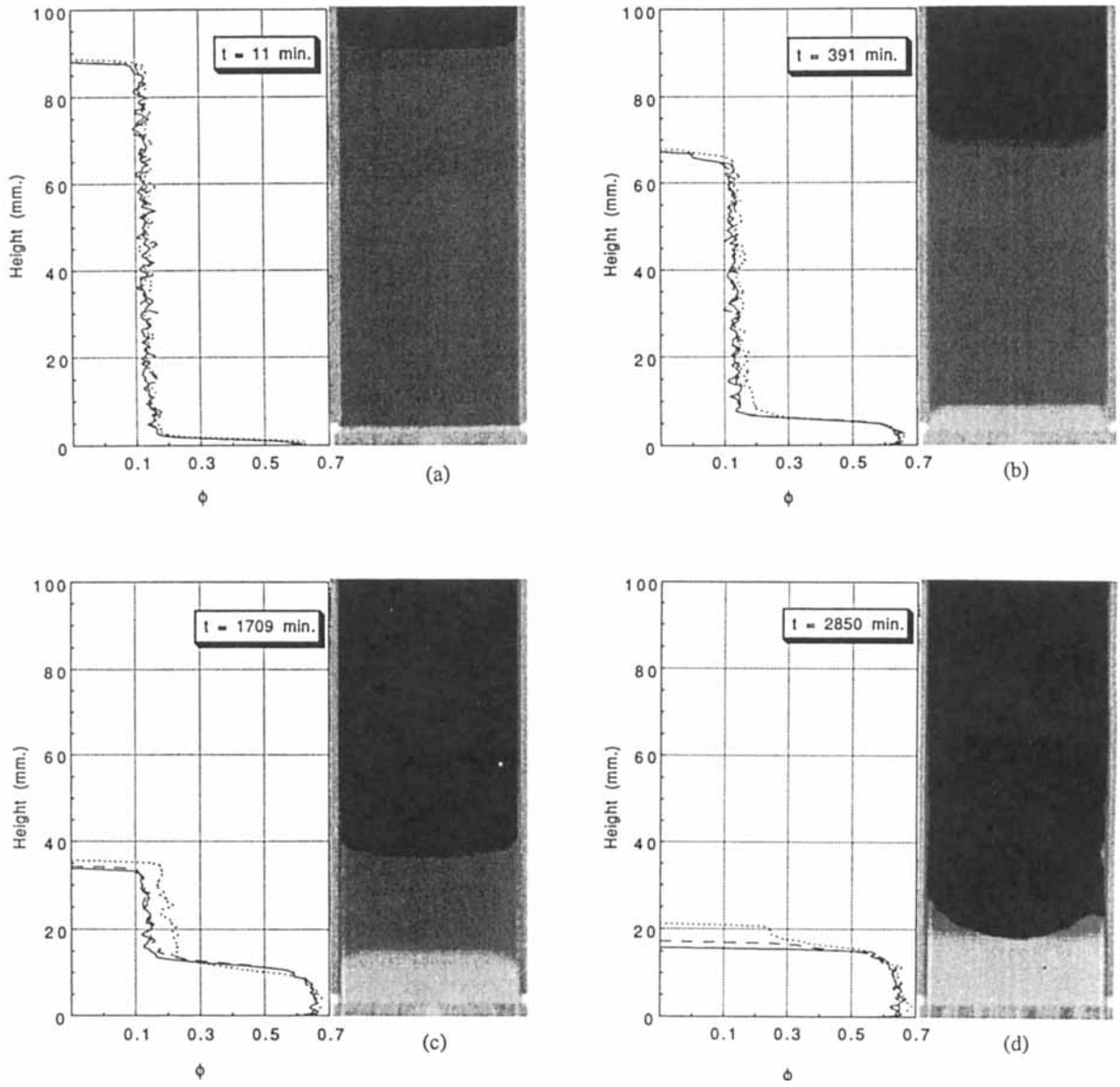

Figure 14. Reconstructed images and associated solid fraction profiles for Experiment D.

— $r/R = 0.000$; - - - - $r/R = 0.430$; · · · · $r/R = 0.817$; where r/R is the ratio of the radial position to the tube radius.

The liquid region grows overnight but the rate is much slower on the second day. As well, substantial axial gradients exist close to the wall in the gel and the cake develops the depression adjacent to the cell wall that was noticed for pliant systems. Finally at the beginning of the third day, a catastrophic separation of the gel from the wall causes the gel to collapse inward upon itself; apparently, separation of the gel from the wall relieves the radial stress gradient. At this point, the experiment was terminated.

Experiment D attempts to circumvent the catastrophic collapse of Experiment C by applying a greater pressure, 1,380 kPa, to a slightly more concentrated dispersion, $\phi_o = 0.13$. Qualitatively, the experiment begins in the same way as Experiment C; a filter cake with an axial solids concentration gradient grows while radial gradients slowly form in the gel, Figure 14. Additionally, the depression in the filter cake near the cell wall forms during the first few hours of filtration, much earlier than in the previous experiments. After five hours, radial cracks appear again and a liquid layer begins to form at the top of the gel. After 24 hours, however, the clear liquid region disappears, leaving only a cake and a gel. The gas/gel interface becomes more curved at later times. These observations manifest themselves more distinctly in the way an experiment is terminated, Figure 14d; the minimum in the gel/gas interface touches the filter cake in the center and gas percolates through, leaving unconsolidated gel regions along the sides.

The solid fraction profiles associated with the images of Figure 14 show significant radial gradients over time, with solids volume fraction as much as 0.05 higher near the tube wall than at the centerline. Clearly, the axial concentration gradient is most accentuated near the cell wall and is hardly noticeable at the centerline. Finally, the centerline interfacial height against time plot, Figure 15, shows a process time ap-

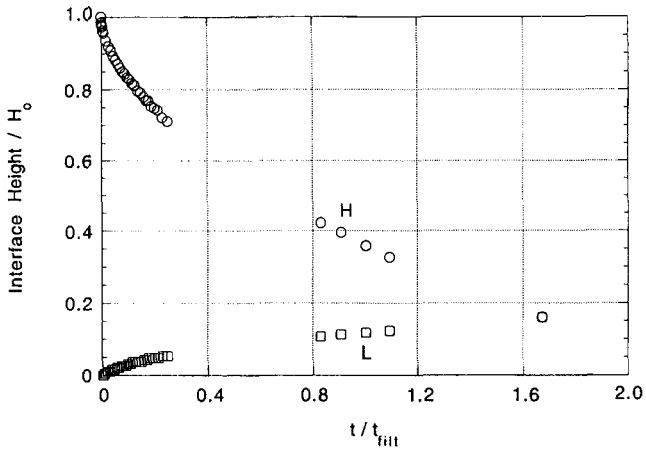

Figure 15. Scaled graph of interface height vs. time at centerline for Experiment D.

proximately 70% longer than the stable case; the lack of a pure solvent layer indicates the lengthening of filtration time is solely due to the network stress.

Wall effects

A point of concern in these experiments involves the effect of gel-wall interactions. Our intention was to minimize wall effects in order to depict purely one-dimensional consolidation. Two steps in the experimental design attempted to accomplish this. First, the cell wall was coated with a teflon spray to promote a perfect slip boundary condition. This minimizes the gel-wall interactions; even then the gel adjacent to the wall ideally feels free slip on one side but is constrained due to particle-particle interactions on the other. Thus, second, a tube with diameter large enough to minimize these effects was designed, hopefully isolating wall effects close to the boundary.

Experiments before and after coating indicate the success of the teflon spray in limiting gel-wall interactions. CAT scans of filtration before teflon coating, Experiment E shown in Figure 16, reveal large fractures, reflecting strong wall-gel interactions. Presumably, the impeded downward movement of gel near the wall creates tension which opens the macroscopic fractures. Figure 17 shows that radial gradients do not develop significantly in the experiment. Trends observed with different combinations of particle size, volume fraction, and temperature indicate that Experiment E would behave pliantly, though its "true" classification is not definitive. Indeed, Experiments A and B at similar conditions, but with the teflon coating, show pliant behavior with weaker wall-gel interactions, attesting to the spray's effectiveness.

Quantitatively, the large diameter of the cell confine the wall effects close to the wall, as depicted by the superposition of concentration profiles for various radial positions in Figures 4, 8, 12, 14 and 16. In fact only for stiff systems do we witness substantial deviations in concentration profiles with radial position. However, from a qualitative perspective, the radial effects can be considerable: the tearing of gel from the wall surface in Experiment C, the large fractures present in Experiment A, and the parabolic interface upon filtration completion in Experiment D.

Though wall effects inevitably play some role in all experiments, the consequences are probably limited for pliant systems in which the wall was coated with teflon. This allows a comparison with previous theories developed for gel consolidation. For stiff systems, however, the various qualitative effects observed indicate a significant coupling of axial consolidation with radial effects. Thus modeling the latter is necessarily more complex.

Comparison with theory

Our results for pliant, strongly flocculated suspensions show features quite different from those predicted by Landman et

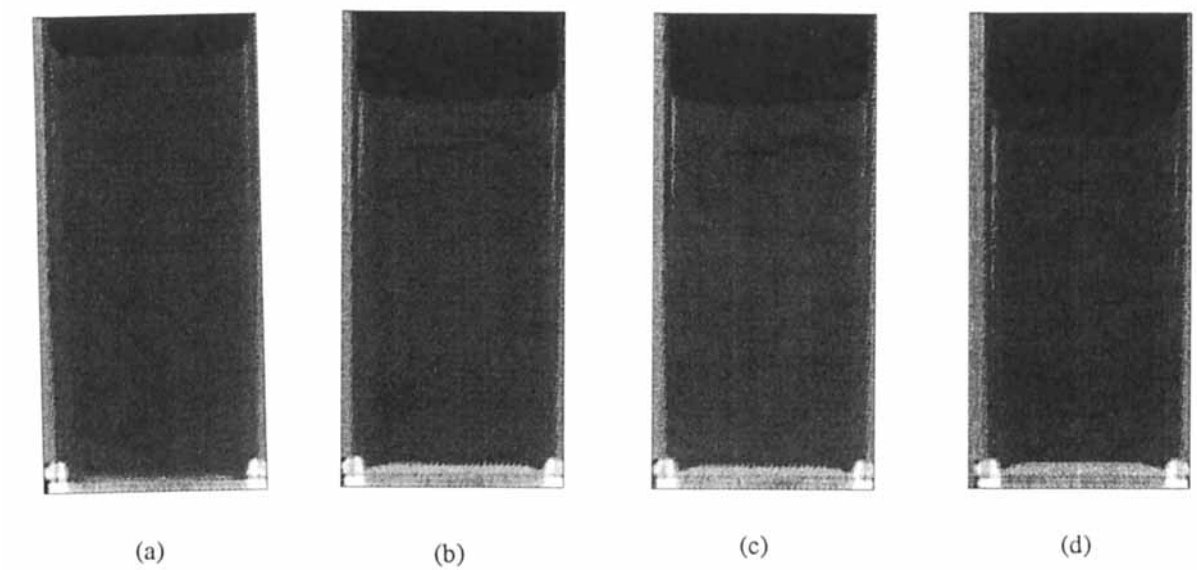

Figure 16. Reconstructed images for Experiment E.

(a) $t = 7$ min; (b) $t = 100$ min; (c) $t = 108$ min; (d) $t = 118$ min.

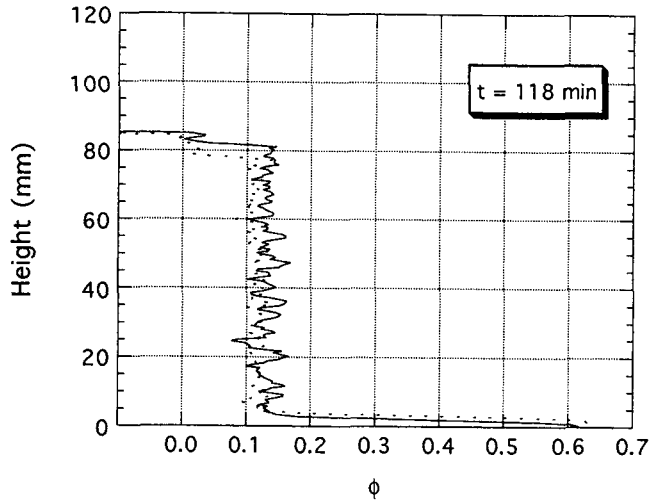

Figure 17. Volume fraction profiles for Experiment E.

— centerline; - - - - $r/R = 0.41$; where r/R is the ratio of the radial position to the tube radius.

al. (1991) using Buscall and White's model. However, their calculations neglect gravitation forces; hence, a clear zone never formed above the dispersion. Recent work by Landman and Russel (1993) redressed the previous solution by incorporating gravity and large values of $\Delta p/\sigma_y(\phi_o)$. Their solutions of Buscall and White's model for pliant systems qualitatively resemble our experimental observations: the formation of a clear zone, the slowing of the pure solvent/gel interface as it approaches the cake surface, and the turnover of the difference height vs. time plot.

A quantitative comparison of the theory with our experiments is easily established. Note that the following development is independent of the forms chosen for $K(\phi)$ and $\sigma_y(\phi)$ and, therefore, provides a test of the model's basic assumptions. Using the appropriate momentum and continuity relations written on the solid and liquid, the solids velocity for pressure filtration equals that for sedimentation plus the superficial velocity of the fluid out the bottom (Landman and Russel, 1993):

$$v = -U_{fl} - U_o K(\phi)\left[1 - \frac{\partial\sigma/\partial x}{\Delta\rho g\phi}\right] \tag{6}$$

where $\partial\sigma/\partial x$ is the local axial stress gradient, v is the local solids velocity, and U_{fl} is the magnitude of the fluid velocity exiting the bottom of the cell.

The model predicts the concentration of the dispersion by distinguishing three regions: a clear zone between an upper interface, H, and a lower one, y, where $\phi = 0$; a uniform zone between y and a location L_c, where $\phi = \phi_o$; and a consolidation zone between L_c and the bottom, where $\phi > \phi_o$. Assuming compression cannot occur unless $\sigma \geq \sigma_y$, L_c to mark the position where the uniform gel begins to yield, that is, $\sigma = \sigma_y(\phi_o)$, and noting that $U_{fl} = -dH/dt$ and $v = dy/dt$, Eq. 6 can be recast as:

$$\frac{d(H-y)}{dt} = U_o K(\phi_o)\left[1 - \frac{\sigma_y(\phi_o)}{\Delta\rho g\phi_o(y - L_c)}\right] \tag{7}$$

Note that L and L_c are not identical; L is generally smaller than L_c and roughly comparable to the point in the consolidating zone where $\partial\phi/\partial x$ is a maximum. The ratio of the yield stress to self-weight of uniform gel controls the difference velocity. Thus, a plot of instantaneous difference velocity against $1/(y - L_c)$ should follow a straight line with an intercept equal to the hindered sedimentation velocity, $U_o K(\phi_o)$, and a slope proportional to the yield stress at the ϕ_o. This expression is valid until $H = y$, at which the theory as formulated by Landman et al. (1991) should describe the consolidation of the remaining gel.

Alternatively, Eq. 7 can be used to interpret difference height vs. time curves, Figures 8 and 12. Assuming the validity of Eq. 7 over the entire range and H_o large enough such that $\sigma_y(\phi_o)/\Delta\rho g\phi_o H_o \ll 1$, the initial slope of the curve reduces to $U_o K(\phi_o)$. The maximum corresponds to the difference velocity set equal to zero; physically, the uniform region's self-weight balances the yield stress at ϕ_o. The corresponding height of uniform gel:

$$y - L_c = \frac{\sigma_y(\phi_o)}{\Delta\rho g\phi_o} \tag{8}$$

permits an estimate of $\sigma_y(\phi_o)$ if $y - L_c$ is identified experimentally. Beyond this point, gravity no longer affects consolidation; the difference velocity is governed by liquid flow through the gel and filter cake. At late times, the difference velocity approaches the limit with $dy/dt = 0$ and dH/dt determined by Darcy flow through the consolidated region. This sets a minimum on the height of the uniform zone as:

$$(y - L_c)_{\min} = \frac{\sigma_y(\phi_o)}{\Delta\rho g\phi_o\left(1 + \dfrac{U_{fl}}{U_o K(\phi_o)}\right)} \tag{9}$$

assuming negligible pressure drop across the uniform zone and a uniform cake density.

Experiments A and B were analyzed within context of the aforementioned interpretation. Interfacial heights were taken as the centerline values, with curves directly fitted to H and y to determine values for the difference velocity. L_c was estimated from individual profiles by discerning the point where ϕ deviates from ϕ_o. Because of the jagged concentration profiles, errors in L_c can be as large as 2.5 mm. However, the difference between y and L_c is not significantly affected until y and L_c are comparable in value. The error bars in Figure 18 are representative of the errors in all plots. Generally, L_c/L was closer to unity than predicted by Landman and Russel (1993) for a particular moment during filtration. Experiment C differs qualitatively in its consolidation; the formation of fractures and a long induction time relative to Experiments A and B points to mechanisms of consolidation not specifically included in the theory as formulated. Thus the corresponding analysis is omitted.

Figure 18 graphs the difference velocity against the reciprocal of the height of the uniform zone for Experiments A and B, with U_o and H_o scaling the quantities, respectively. The dominant feature is an initial linear region followed by a sharp transition to an apparently zero slope. In reality, L_c jumps up to coincide with y, indicating that the entire gel region is con-

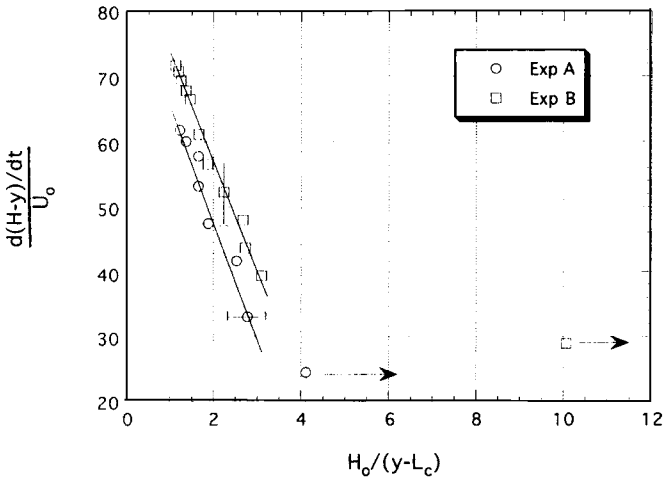

Figure 18. Difference height velocity vs. reciprocal of uniform zone height.

solidating, while the difference velocity continues to fall. This contradicts the expectation that a steady uniform gel region should establish itself late in the experiment. Additionally, y equals L_c long before the maximum in the corresponding difference height vs. time plot is reached. Thus an interpretation of the experiments in terms of the difference height vs. time plots is invalid.

Nonetheless, the early time linear regions of Figure 18 can be analyzed in terms of Eq. 7. Table 4 presents the quantities computed. Experiments A and B show values of $K(\phi_o)$ and the yield stress at ϕ_o which are consistent with their respective experimental conditions and each other. In general, the values of $\sigma_y(\phi_o)$ are in accord with those found by Auzerais et al. (1990). The values of $(y-L_c)_{\min}$, calculated from experimental observables and Eq. 9, indicate that a uniform gel region, of height detectable by the CAT scanner, should have been observed.

A better sense of the deviations from theoretical expectations can be obtained by examining Figure 19. The plot of difference velocity normalized on U_o vs. $(y-L_c)/H_o$ shows experimental data, in the form of data points, and theoretical curves, based on extending the linear regions of Figure 18. At early times the gel consolidates in accord with the theory. Later, however, consolidation in the uniform gel region continues until the region is no longer measurable, while the theory predicts that consolidation should slow and the region should be preserved to a steady height indicated by the left endpoints of the theoretical curves of Figure 19. This raises the question of whether a compressive yield stress actually exists in these dispersions.

Discussion

Our results for pliant cases show many features which are predicted by the network model as identified by Landman and Russel (1993): the formation of a clear zone; the early square root of time dependence for the interfacial heights; the formation of a dense filter cake which obeys Darcy's law; and slowing of gel consolidation near the end of the process. Indeed, the qualitative agreement encourages the implementation of the full solution, which we will pursue in a later article.

Table 4. Dispersion Physical Properties: Measured and Calculated

Exp.	U_o (mm/s)	$K(\phi_o)$	$\sigma_y(\phi_o)$ (kPa)	$[\sigma_y(\phi_o)]/(\Delta\rho g H_o\phi_o)$	$(y-L_c)_{\min}$ (mm)
A	2.31×10^{-5}	83	1.7	0.214	5.4
B	2.18×10^{-5}	89	1.5	0.185	8.5

In lieu of this, significant conclusions can still be drawn. The observed consolidation throughout the uniform gel region for pliant systems is inconsistent with the notion that compression occurs only when the interparticle stress exceeds the local value of the yield stress. Experiments conducted to check whether syneresis or a similar thermodynamic force contributed to mechanical consolidation showed no such effect. One possible explanation is that an additional mechanism, such as stress-induced creep, enhances consolidation. Such a mechanism would also help explain the differences observed between Experiments C and D, which differ only in the applied pressure. However, such an idea has yet to be scrutinized carefully.

Clearly, the radial gradients in ϕ for stiff systems lie beyond this unidimensional model. The confinement of this effect close to the wall, however, may allow some agreement with the theory, as formulated by Landman et al. (1991) in the center region though the assumption of a compressive yield stress would require rectification. Besides the stronger presence of radial gradients in ϕ, however, the observed phenomena of macroscopic fracturing and consolidation in stiff systems is not accounted for in Buscall and White's formulation. Their unidimensional development considers a purely plastic, consolidating mode of deformation. Fracturing necessitates some type of extensional motion which overcomes elasticity. Though the majority of fractures are isolated near the cell wall, the assumption that the center section acts as a purely consolidating plastic is not founded at the present moment. As well, the tension which induces fracturing probably originates radially from the gel/wall interaction, necessitating a two-dimensional model. These considerations compose some issues to be addressed by future work.

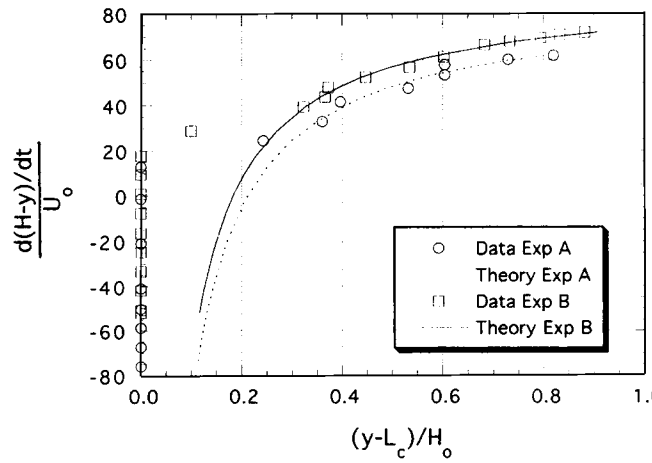

Figure 19. Difference height velocity vs. uniform zone height.

Acknowledgments

We wish to thank Mr. Archie Harkness in helping design the filtration cells and Ms. Brenda Schmidt for her aid in operating the CAT scanner. Additionally, we thank Schlumberger-Doll Research Laboratories for their generosity in allowing us access to their scanner. This work was supported by grant DE-FG02-85ER45210 of the Dept. of Energy's Office of Basic Energy Sciences.

Notation

a = particle radius
C_F = coefficient of consolidation
E = photon energy
g = gravitational force constant
H = gas/pure solvent interface position
H_o = gas/pure solvent interface initial position
I = intensity of scattered photons
I_o = initial intensity of photons
k = permeability
$K(\phi)$ = hindered settling coefficient
L = filter cake height
L_c = bottom of constant ϕ gel region
L_f = final filter cake height
t = time
t_{filt} = filtration time-scale
t_{sed} = sedimentation time-scale
U_o = Stokes settling velocity of an isolated sphere
y = pure solvent/gel interface position
Z = effective atomic number

Greek letters

α = photoelectric effect parameter
β = Compton scattering parameter
Δp = applied pressure
$\Delta\rho$ = density difference between solid and liquid
η = pure solvent viscosity
μ = linear attenuation coefficient
μ_c = linear attenuation coefficient due to Compton scattering
μ_m = measured linear attenuation coefficient
μ_p = linear attenuation coefficient due to photoelectric effect
μ_r = reference material linear attenuation coefficient
ρ = bulk density
ρ_f = fluid density
σ = network stress
σ_y = compressive yield stress
ϕ = solids volume fraction
ϕ_m = maximum solids volume fraction in filter cake
ϕ_o = initial gel solids volume fraction

Literature Cited

Auzerais, F. M., R. Jackson, and W. B. Russel, "The Resolution of Shocks and the Effects of Compressible Sediments in Transient Settling," *J. Fluid Mech.*, **195**, 437 (1988).

Auzerais, F. M., "The Transient Settling of Stable and Flocculated Dispersions," PhD Thesis, Princeton Univ. (1988).

Auzerais, F. M., R. Jackson, W. B. Russel, and W. F. Murphy, "The Transient Settling of Stable and Flocculated Dispersions," *J. Fluid Mech.*, **221**, 613 (1990).

Badley, R. D., W. T. Ford, F. J. McEnroe, and R. A. Assink, "Surface Modification of Colloidal Silica," *Langmuir*, **6**, 792 (1990).

Baxter, R. J., "Percus-Yevick Equation for Hard Spheres with Surface Adhesion," *J. Chem. Phys.*, **49**, 2770 (1968).

Been, K., and G. G. Sills, "Self-Weight Consolidation of Soft Soils: An Experimental and Theoretical Study," *Geotechnique*, **31**, 519 (1981).

Bergström, L., "Sedimentation of Flocculated Alumina Suspensions: Gamma-Ray Measurements and Comparison to Model Predictions," *J. Chem. Soc. Farad. Trans.*, **88**, 3201 (1992).

Bogush, G. H., M. A. Tracey, and C. F. Zukoski IV, "Preparation of Monodisperse Silica Particles: Control of Size and Mass Fraction," *J. Non-Cryst. Solids*, **104**, 95 (1988).

Bogush, G. H., and C. F. Zukoski IV, "Studies of the Kinetics of the Precipitation of Uniform Silica Particles through the Hydrolysis and Condensation of Silicon Alkoxides," *J. Colloid Interf. Sci.*, **142**, 1 (1991a).

Bogush, G. H., and C. F. Zukoski IV, "Uniform Silica Particle Precipitation: An Aggregative Growth Model," *J. Colloid Interf. Sci.*, **142**, 19 (1991b).

Brooks, R. A., and G. DiChiro, "Principles of Computer Assisted Tomography (CAT) in Radiographic and Radioisotopic Imaging," *Phys. Med. Biol.*, **21**, 689 (1976).

Buscall, R., and L. R. White, "The Consolidation of Concentrated Suspensions," *J. Chem. Soc., Farad. Trans. 1*, **83**, 873 (1987).

Carslaw, H. S., and J. C. Jaeger, *Conduction of Heat in Solids*, Oxford University Press, London (1959).

Chen, M., and W. B. Russel, "Colloidal Silica Gels: Transition and Elasticity," *J. Colloid Interf. Sci.*, **141**, 564 (1990).

Chen, M., "Colloidal Silica Gels: Transition and Elasticity," PhD Thesis, Princeton Univ. (1992).

Chen, M., and W. B. Russel, "On the Volume Fraction Dependence of Elastic Moduli and Transition Temperatures for Colloidal Silica Gels," *Phys. Rev. E*, **47**, 2606 (1993).

Coe, H. S., and G. H. Clevenger, "Methods for Determining the Capacities of Slime-Settling Tanks," *Trans. AIME*, **55**, 356 (1916).

Coenen, S., and C. G. deKruif, "Synthesis and Growth of Colloidal Silica Particles," *J. Colloid Interf. Sci.*, **124**, 104 (1988).

Cormack, A. M., "Reconstruction of Densities from their Projections, with Applications in Radiological Physics," *Phys. Med. Biol.*, **18**, 195 (1973).

Cosgrove, T., N. Finch, B. Vincent, and J. Webster, "The Adsorption of Random Copolymers of Vinyl Acetate and Ethylene on Surface-Modified Silica Particles," *Colloids Surf.*, **31**, 33 (1988).

Davis, K. E., "Sedimentation and Crystallization of Hard-Sphere Colloidal Suspensions: Theory and Experiment," PhD Thesis, Princeton University (1989).

deKruif, C. G., and J. C. van Miltenburg, "Phase Transitions in Sterically Stabilized Silica Colloids Studied by Adiabatic Calorimetry," *J. Chem. Phys.*, **93**, 6865 (1990).

Emmett, S., S. D. Lubetkin, and B. Vincent, "The Growth of Ordered Sediments of Monodispersed Hydrophobic Silica Particles," *Colloids Surf.*, **42**, 139 (1989).

Evans, R. D., *The Atomic Nucleus*, McGraw Hill, New York (1955).

Fitch, B., "Kynch Theory and Compression Zones," *AIChE J.*, **29**, 940 (1983).

Gaudin, A. M., M. C. Fuerstenau, and S. R. Mitchell, "Effect of Pulp Depth and Initial Pulp Density in Batch Thickening," *Mining Eng.*, 613 (June, 1959).

Gibson, R. E., G. L. England, and M. J. L. Hussey, "The Theory of One-Dimensional Consolidation of Saturated Clays," *Geotechnique*, **17**, 263 (1967).

Harris, M. T., R. R. Brunson, and C. H. Byers, "The Base-Catalyzed Hydrolysis and Condensation Reactions of Dilute and Concentrated TEOS Solutions," *J. Non-Cryst. Solids*, **121**, 397 (1990).

Howells, I., K. Landman, A. Panjkov, C. Sirakoff, and L. R. White, "Time-Dependent Batch Settling of Flocculated Suspensions," *Appl. Math. Model*, **14**, 77 (1990).

Iler, R., *The Chemistry of Silica*, Wiley, New York (1979).

Jansen, J. W., C. G. deKruif, and A. Vrij, "Attractions in Sterically Stabilized Silica Dispersions: II. Experiments on Phase Separation Induced by Temperature Variation," *J. Colloid Interf. Sci.*, **114**, 481 (1986).

Karmakar, B., G. De, D. Kundu, and D. Ganguli, "Silica Microspheres from the System Tetraethyl Orthosilicate-Acetic Acid-Water," *J. Non-Cryst. Solids*, **135**, 29 (1991).

Kim, S., and C. F. Zukoski, "A Model of Growth by Hetero-Coagulation in Seeded Colloidal Dispersions," *J. Colloid Interf. Sci.*, **139**, 198 (1990).

Kos, P., "Fundamentals of Gravity Thickening," *Chem. Eng. Prog.*, **73**, 99 (1977).

Kynch, G. H., "A Theory of Sedimentation," *Trans. Farad. Soc.*, **48**, 166 (1952).

LaMer, V. K., and R. H. Dinegar, "Theory, Production and Mechanism of Formation of Monodispersed Hydrosols," *J. Amer. Chem. Soc.*, **72**, 4847 (1950).

Landman, K. A., L. R. White, and R. Buscall, "The Continuous-

Flow Gravity Thickener: Steady State Behavior," *AIChE J.*, **34**, 2 (1988).
Landman, K. A., C. Sirakoff, and L. R. White, "Dewatering of Flocculated Suspensions by Pressure Filtration," *Phys. Fluids A*, **3**, 1495 (1991).
Landman, K. A., and W. B. Russel, "Filtration at Large Pressures for Strongly Flocculated Suspensions," *Phys. Fluids A*, **5**, 550 (1993).
Lange, F. F., and K. T. Miller, "Pressure Filtration: Consolidation Kinetics and Mechanics," *Am. Ceram. Soc. Bull.*, **66**, 1498 (1987).
LeCloux, A. J., J. Bronckart, F. Noville, C. Dodet, P. Marchot, and J. P. Pirard, "Study of the Texture of Monodisperse Silica Sphere Samples in the Nanometer Size Range," *Colloids Surf.*, **19**, 359 (1986).
Lee, K., and G. C. Sills, "The Consolidation of a Soil Stratum, Including Self-Weight Effects and Large Strains," *Numerical & Analyt. Meth. Geomech.*, **5**, 405 (1981).
Look, J., G. H. Bogush, and C. F. Zukoski, "Colloidal Interactions during the Precipitation of Uniform Submicrometre Particles," *Farad. Discuss. Chem. Soc.*, **90**, 345 (1990).
Massuda, M., K. Bridger, M. Harvey, and F. M. Tiller, "Filtration Behavior of Slurries with Varying Compressibilities," *Sep. Sci. Tech.*, **23**, 2159 (1988).
Matijević, E., "Production of Monodisperse Colloidal Particles," *Ann. Rev. Mater. Sci.*, **15**, 483 (1985).
Matsoukas, T., and E. Gulari, "Dynamics of Growth of Silica Particles from Ammonia-Catalyzed Hydrolysis of Tetra-ethyl-orthosilicate," *J. Colloid Interf. Sci.*, **124**, 252 (1988).
Matsoukas, T., and E. Gulari, "Monomer-Addition Growth with a Slow Initiation Step: A Growth Model for Silica Particles from Alkoxides," *J. Colloid Interf. Sci.*, **132**, 13 (1989).
Michaels, A. S., and J. C. Bolger, "Settling Rates and Sediment Volumes of Flocculated Kaolin Suspensions," *Ind. Eng. Chem. Fund.*, **1**, 24 (1962).
Osseo-Asare, K., and F. J. Arriagada, "Preparation of SiO_2 Nanoparticles in a Non-Ionic Reverse Micellar System," *Colloids Surf.*, **50**, 321 (1990).
Pathmamanoharan, C., "Preparation of Monodisperse Polyisobutene Grafted Silica Dispersions," *Colloids Surf.*, **34**, 81 (1988/89).
Philipse, A. P., and A. Vrij, "Preparation and Properties of Nonaqueous Model Dispersions of Chemically Modified, Charger Silica Spheres," *J. Colloid Interf. Sci.*, **128**, 121 (1989).
Post, A. J., personal communication (1985).
Shin, B. S., and R. I. Dick, "Applicability of Kynch Theory to Flocculent Suspensions," *J. Environ. Eng. Div. Am. Soc. Civ. Eng.*, **106**, 505 (1980).
Shirato, M., H. Kato, K. Kobayashi, and H. Sakazaki, "Analysis of Settling of Thick Slurries Due to Consolidation," *J. of Chem. Eng. Jap.*, **3**, 98 (1970).
Stöber, W., A. Fink, and E. Bohn, "Controlled Growth of Monodisperse Silica Spheres in the Micron Size Range," *J. Colloid Interf. Sci.*, **26**, 62 (1968).
Tan, C. G., B. D. Bowen, and N. Epstein, "Production of Monodisperse Colloidal Silica Spheres: Effect of Temperature," *J. Colloid Interf. Sci.*, **118**, 290 (1987).
Terzaghi, K., and R. B. Peck, *Soil Mechanics in Engineering Practice*, Wiley, New York (1948).
Tiller, F. M., and Z. Khatib, "The Theory of Sediment Volumes of Compressible, Particulate Structures," *J. Colloid Interf. Sci.*, **100**, 55 (1984).
Tjipangandjara, K. F., Y. B. Huang, P. Somasundaran, and N. J. Turro, "Correlation of Alumina Flocculation with Adsorbed Polyacrylic Acid Conformation," *Colloids Surf.*, **44**, 229 (1990).
Tory, E. M., and P. T. Shannon, "Reappraisal of the Concept of Settling in Compression," *Ind. Eng. Fund.*, **4**, 194 (1965).
van Duijneveldt, J. S., and D. Beysens, "Adsorption on Colloids and Flocculation: The Influence of Salt," *J. Chem. Phys.*, **94**, 5222 (1991).
Van Helden, A. K., J. W. Jansen, and A. Vrij, "Preparation and Characterization of Spherical Monodisperese Silica Dispersions in Nonaqueous Solvents," *J. Colloid Interf. Sci.*, **81**, 354 (1981).
Vrij, A., M. H. G. M. Penders, P. W. Rouw, C. G. deKruif, J. K. G. Dhont, C. Smits, and H. N. W. Lekkerkerker, "Phase-transition Phenomena in Colloidal Systems with Attractive and Repulsive Particle Interactions," *Faraday Discuss. Chem. Soc.*, **90**, 31 (1990).
Wellington, S. L., and H. J. Vinegar, "X-Ray Computerized Tomography," *J. Pet. Tech.*, 885 (Aug., 1987).
Yagi, S., and Y. Yamazaki, "Fundamental Studies on the Settling of Suspensions," *J. Chem. Eng. Japan*, **24**(2), 81 (1960).

Manuscript received May 13, 1993, and revision received Nov. 3, 1993.